



**HAL**  
open science

## Small body harvest with the Antarctic Search for Transiting Exoplanets (ASTEP) project

S N Hasler, A Y Burdanov, J de Wit, G Dransfield, L Abe, A Agabi, P Bendjoya, N Crouzet, T Guillot, D Mékarnia, et al.

► **To cite this version:**

S N Hasler, A Y Burdanov, J de Wit, G Dransfield, L Abe, et al.. Small body harvest with the Antarctic Search for Transiting Exoplanets (ASTEP) project. Monthly Notices of the Royal Astronomical Society, 2023, 526 (3), pp.3601-3609. 10.1093/mnras/stad2943 . hal-04532654

**HAL Id: hal-04532654**

**<https://hal.science/hal-04532654v1>**

Submitted on 4 Apr 2024



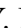




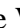

















**HAL** is a multi-disciplinary open access archive for the deposit and dissemination of scientific research documents, whether they are published or not. The documents may come from teaching and research institutions in France or abroad, or from public or private research centers.

L'archive ouverte pluridisciplinaire **HAL**, est destinée au dépôt et à la diffusion de documents scientifiques de niveau recherche, publiés ou non, émanant des établissements d'enseignement et de recherche français ou étrangers, des laboratoires publics ou privés.



Distributed under a Creative Commons Attribution 4.0 International License

# Small body harvest with the Antarctic Search for Transiting Exoplanets (ASTEP) project

S. N. Hasler<sup>1</sup>                                            

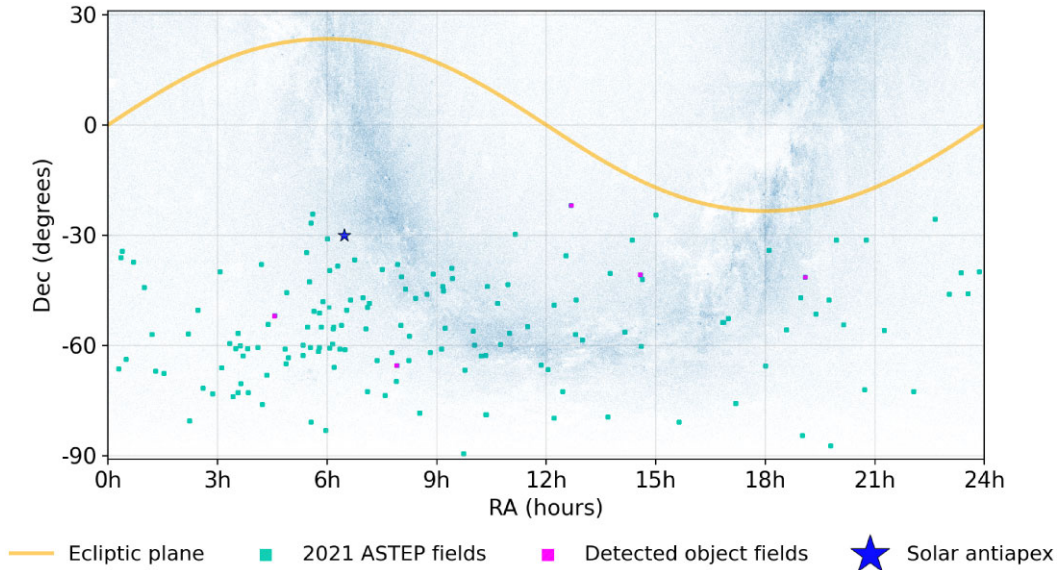


**Figure 1.** Projection of the celestial sphere with stars (blue dots) from the *Tycho-2* catalogue (Høg et al. 2000), the ecliptic plane (orange line), the solar antiapex (blue star), and the processed ASTEP fields (teal squares) overlaid. Fields with detections of known objects are also shown in magenta. The size of the markers depicts the size of ASTEP’s FoV.

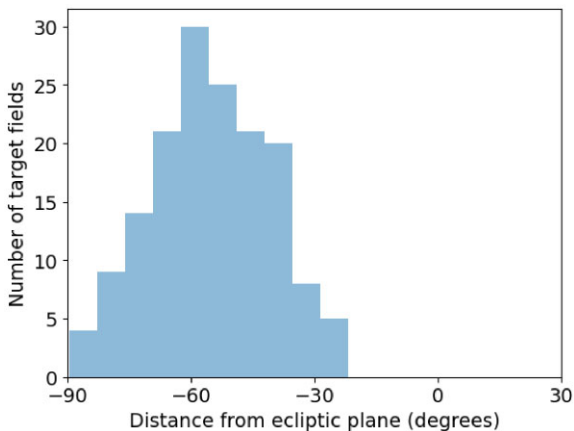


**Figure 2.** Distribution of observed target fields for the 2021 ASTEP 400 observations with respect to the ecliptic plane.

continuous three month long night during the Antarctic winter months, which allows for longer observations than can be obtained by standard mid-latitude surveys.

ASTEP’s location (latitude  $-75^{\circ}06'01''.3$ , longitude  $123^{\circ}19'26''.5$ , elevation 3267 m) makes it particularly unique for several other reasons, including that it has been the only photometric survey operating continuously for several years on the Antarctic continent. Other instruments include the Infrared Telescope Maffei also at Concordia (Tosti et al. 2003; Durand et al. 2014), the Antarctica Schmidt Telescopes (AST3) at the non-manned Kunlun station, Dome A (Yuan et al. 2014), and the Multi-band Survey Telescope at the Zhongshan Station on the coast of Antarctica (Chen et al. 2023). The ASTEP project began in 2006 and the first observations of the ASTEP 400 telescope began in 2010 (Daban et al. 2010; Guillot et al. 2015; Mékarnia et al. 2016).

ASTEP’s vantage point from Antarctica is mostly away from the ecliptic, and also covers the region on the sky containing the solar antiapex (see Figures 1 and 2). Hoover, Seligman & Payne (2022)

suggest that the ISO population is characterized by a clustering of trajectories in the direction of the solar apex and antiapex (the solar apex refers to the direction that the Sun travels with respect to the local standard of rest, with the antiapex directly opposite). ASTEP’s point of view provides the potential to observe ISOs, should they enter the Solar system from the direction of the antiapex. Additionally, ASTEP’s range of view may be uniquely suited to catch higher inclination small bodies, whose evolutionary history are not yet well understood (Hromakina et al. 2021). Serendipitous detections of small bodies in the ASTEP data could thus provide better context for these groups if they happen to cross its FoV.

The rest of this paper is organized as follows, Section 2 describes the ASTEP project and the data it provides. Section 3 discusses the original data processing pipeline and changes made to process ASTEP data. In Section 4, we discuss the application of the pipeline to 1 yr of ASTEP data. We summarize the findings of this work and discuss future applications in Section 5.

## 2 ASTEP DATA

The ASTEP project was designed to assess the ability to perform high-precision photometry to search for transiting exoplanets at Dome C, Antarctica (Crouzet et al. 2011) with ASTEP 400, a 40-cm telescope with a  $1^{\circ} \times 1^{\circ}$  FoV (Daban et al. 2010; Guillot et al. 2015). Since, ASTEP has produced a number of observations and detections of difficult exoplanet transits, particularly of systems with long orbital periods and transit timing variations (such as Burt et al. 2021; Dransfield et al. 2022a; Trifonov et al. 2023). The unique location of the ASTEP observatories offers prime observing conditions for ground-based photometry, given an exceptionally clear sky, great seeing conditions, and near-uninterrupted observations during the 3 month long Antarctic winter (Crouzet et al. 2010; Crouzet et al. 2018). In 2022, ASTEP was moved to another astronomic dome on the Concordia station and upgraded to have the ability to perform simultaneous two-colour photometry (Crouzet et al. 2020; Schmider et al. 2022; Dransfield et al. 2022b).

ASTEP 400 is a fully computer-controlled telescope. Observations are conducted in an automatic observation mode, or remotely operated when needed, from the beginning of March up to the end of September for each campaign. Data acquisitions are performed when the Sun elevation is lower than  $-8^\circ$ . During each campaign, more than 150 science fields are observed for a total of  $\sim 2000$  h of science exposure frames corresponding to about 5 TB of data. At the time of writing, the programme has collected about 50 TB of data overall. The aim of this work is to begin maximizing the science return of this data by recovering serendipitous detections of small bodies that cross the FoV.

The data acquired for this work comprises one season of observations from the ASTEP 400 telescope (MPC code P48), from 2021 March to October (see Fig. 1). The data are comprised of 135 351 images from 167 target fields. The ASTEP target fields from 2021 consist primarily of *TESS* (Transiting Exoplanet Survey Satellite) follow-up candidates. Images were taken with the FLI Proline science camera with  $4k \times 4k$  pixels and a pixel scale of  $0.9$  arcsec  $\text{pixel}^{-1}$ . A dichroic plate split the light for guiding and science, into  $< 600$  nm and  $> 600$  nm, respectively. Images were taken without a filter on the science camera, resulting in a bandpass of 600–800 nm. This is close to the R Johnson–Cousins passband, and is thus designated as the ‘R’ filter. Image exposure times range from 2 to 200 s.

After removing defocused fields from the 2021 observations of bright targets (e.g.  $\beta$  Pictoris and HD 42933), we were left with 141 unique target fields for processing across 206 nights. This translates to 141 square degrees of sky coverage over the course of the observing season. The average observation duration per target was just over 4 h, with the longest observation duration being  $\sim 13$  h. The data for the 206 nights were then passed through our data processing pipeline (see Section 3).

### 3 DATA PROCESSING PIPELINE

We developed a data processing and analysis pipeline, described in B23, to recover serendipitous detections of small bodies in a ground-based photometric survey. The pipeline is designed to employ a publicly-available, GPU-accelerated synthetic tracking software, TYCHO TRACKER (Parrott 2020). The framework was initially tested and applied to data from the SPECULOOS survey, a targeted ground-based photometric survey searching for transiting planets around the nearest ultra-cool dwarf stars. The application of the framework to the SPECULOOS data and results are described in B23.

The pipeline structure is nearly identical to the structure described in B23, with minor changes made to account for the ASTEP data structure. The pipeline is coded in PYTHON programming language, except the synthetic tracker, and run on a computer with a WINDOWS 10 operating system. The synthetic tracking portion happens in TYCHO TRACKER and uses OPENCL to communicate with the GPUs. A description of the pipeline and the updates made to process the ASTEP data is given in the following sections.

#### 3.1 ASTEP data pipeline

The ASTEP data used for this work was provided as raw FITS files that must be calibrated and corrected accordingly before being passed to the synthetic tracker. Calibration was performed using standard bias and dark corrections. The ASTEP data do not provide flat-fields because it is not easy to gather twilight flats in their location and dome flats are not available, so we did not apply any flat-field correction during the calibration step of this work. We then perform additional correction steps to mask and remove bad

pixels and defective columns from the science images. The pipeline also performs source extraction on the images for filtering. This process utilizes an image segmentation technique from PHOTUTILS, an ASTROPY affiliated PYTHON package. More information on the removal of poor quality and defocused images can be found in B23. Affected images may include those that were taken in a defocused mode when ASTEP was observing a bright star (e.g. observations of the  $\beta$  Pictoris target field).

From mid-July to early September of 2021, an issue that prevented the shutter from closing on ASTEP rendered the bias and dark images unusable (Triaud private communication). We separated 22 nights in the data from mid-July to early September that were affected by this issue by measuring the mean and standard deviation of the counts in the bias and dark images. These nights were processed by the pipeline without the bias and dark correction step.

Calibrated and filtered images are then checked for relatively even gaps in observation time between each image. After filtering, it is possible that bad images have been removed intermittently, causing uneven gaps in overhead. These uneven or large gaps in time significantly reduce the speed at which TYCHO TRACKER is able to process a field of observations. Large gaps in time mean there are more object search vectors that need to be considered. If the ASTEP images have large gaps between observations, they are separated into groups at each gap to minimize computational time.

As with the original pipeline, calibrated and filtered images are then passed to the synthetic tracker in groups. Images are aligned and processed by the synthetic tracker. After the shifting and stacking process, assuming objects are moving linearly on the FoV, TYCHO TRACKER returns parameters for any object candidates that may have been identified in the sequence of images. It outputs a set of tracks, or candidate detections, with information about their speed, position angle (PA), pixel coordinates, and the signal-to-noise ratio (S/N) of the detection. This information is cross-checked with the Minor Planet Center (MPC) data base of small body orbits and the FIND\_ORB<sup>3</sup> software to report previously known objects. Coordinates of both known and unknown candidate objects are recorded and can then be submitted to the MPC after review. For further details on this process, see B23.

#### 3.2 Sensitivity tests

To gather an understanding of how well the pipeline retrieved objects from the ASTEP data, we conducted detection efficiency tests using the NASA Jet Propulsion Laboratory (JPL) Small-Body Identification<sup>4</sup> Application Program Interface (API). We compared our fields with detections to all of the known objects that were present in the FoVs to recover the retrieval rate of our pipeline. The results of our tests are described in detail in Section 4.

We also performed injection-retrieval tests on the fields with detected known objects. We injected 100 synthetic moving objects into each set of FITS files prior to calibration for nights with known object detections. The synthetic object injection module is described in detail in B23. Fields with injected objects were processed by the pipeline and the detected objects were compared with the injected ones. The results agree with the detection efficiency tests above and are described in Section 4.

<sup>3</sup>[https://www.projectpluto.com/find\\_orb.htm](https://www.projectpluto.com/find_orb.htm) (Accessed 31 May 2023)

<sup>4</sup>[https://ssd-api.jpl.nasa.gov/doc/sb\\_ident.html](https://ssd-api.jpl.nasa.gov/doc/sb_ident.html) (Accessed 20 May 2023)

**Table 1.** All processed target fields. Fields with known small body detections are listed first, followed by fields with no detections. Latitude and longitude coordinates are in the geocentric mean ecliptic reference frame. Undetected known objects are listed down to the faintest  $V_{\text{mag}}$  detected in the target fields with known object detections. The full table is available online.

Target name	Ecliptic longitude (deg)	Ecliptic latitude (deg)	RA (hms)	Dec. (dms)	Filter	Observed hours	Detected known objects	Undetected known objects	Faintest $V_{\text{mag}}$
TOI-772	198.117	-16.049	12 40 46	-21 52 22	<i>R</i>	15.3	14	11	20.4
TOI-1955	43.157	-71.902	04 33 40	-51 57 22	<i>R</i>	1.7	1	1	19.0
TOI-823	229.541	-24.235	14 34 38	-40 44 23	<i>R</i>	7.8	2	2	18.6
TOI-283	187.709	-78.424	07 54 17	-65 26 29	<i>R</i>	9.0	1	1	17.0
TOI-1130	282.800	-18.729	19 05 30	-41 26 15	<i>R</i>	7.7	2	4	18.8
HD1397b	319.958	-58.526	00 17 47	-66 21 32	<i>R</i>	4.4	–	–	–
HD37781	77.569	-73.848	05 38 17	-50 38 27	<i>R</i>	4.2	–	–	–
TOI-1027	181.303	-32.063	11 08 32	-29 39 11	<i>R</i>	6.8	–	–	–
TOI-1041	177.183	-64.697	09 13 36	-55 11 52	<i>R</i>	1.0	–	–	–
TOI-1054	291.765	-33.280	20 08 27	-54 19 03	<i>R</i>	2.1	–	–	–

**Table 2.** Objects detected in each of the five target fields and their corresponding magnitudes, orbit groupings, and object numbers. Orbit grouping and absolute magnitude ( $H$ ) for each object were retrieved from the JPL Horizons Database.

Object name	Object number	Orbit grouping	Visual magnitude	Absolute magnitude	Target field
2001 VJ46	194 412	MBA	19	15.61	TOI-772
2013 AZ119	542 241	MBA	20	17.67	TOI-772
2001 OK69	618 481	MBA	20	16.38	TOI-772
2010 TZ18	264 237	MBA	15.5	15.84	TOI-772
Tuchkova	3803	MBA	15.1	11.33	TOI-772
2001 OD25	63 471	MBA	19.3	15.08	TOI-772
2012 DH7	454 003	MBA	20	16.65	TOI-772
2001 OA108	54 941	MBA	17.5	13.37	TOI-772
2000 RC88	62 087	MBA	18.3	14.44	TOI-772
2012 HO39	459 337	MBA	19.6	17.14	TOI-772
2012 JG36	542 029	MBA	19.8	16.30	TOI-772
2004 XG58	230 948	MBA	20.4	15.80	TOI-772
2004 XX97	198 521	MBA	20.2	15.85	TOI-772
2001 VV89	111 121	MBA	18	14.14	TOI-772
2005 EH243	299 140	Hungaria	19	17.85	TOI-1955
1998 WK1	137 063	MBA	18.4	14.86	TOI-823
1999 TV264	237 453	MBA	18.6	14.34	TOI-823
2000 GL81	81 393	MBA	18.8	12.70	TOI-1130
1999 GN33	101 788	MBA	18.4	16.08	TOI-1130
C/2019 T2		Comet	18	13.92	TOI-283

## 4 RESULTS AND DISCUSSION

We analysed observations from the ASTEP 400 telescope from 206 nights in 2021, with dates between 2021 March 1 and 2021 October 5, which included 165 total target fields, with 141 unique targets. The average duration of observations was  $\sim 4$  h. No new, unknown moving objects were discovered, but we detected previously known objects in 5 of the fields across 6 of the observing nights. All target fields from 2021 are shown in Fig. 1 and Table 1. Target fields with detected objects are also indicated in Table 1 and shown in magenta in Fig. 1.

All detected objects are listed in Table 2, along with their corresponding numbers, magnitudes, orbit groupings, and the fields in which they were recovered. The detected objects span several dynamical classes, including one inner main-belt (IMB) asteroid of the Hungaria group, 18 main-belt asteroids (MBAs), and one comet (see Table 3 for dynamical class definitions). The dynamical classes of the bodies were retrieved from the JPL Horizons Database<sup>5</sup> The

**Table 3.** The orbital elements of groups of small bodies as defined by the JPL Horizons Database, where  $a$  is the semimajor axis (au),  $q$  is the perihelion distance (au), and  $Q$  is the aphelion distance (au).

Orbital grouping	Orbital parameters
Inner Main-belt Asteroid	$a < 2.0, q > 1.666$
Main-belt Asteroid	$2.0 < a < 3.2, q > 1.666$
Comet-like	$Q > 5.0$

speed and apparent angular rate on the plane of sky for each of these objects is presented Fig. 3; their  $V_{\text{mag}}$  distribution is presented in Fig. 4.

The speeds of the detected objects range from the slowest moving detection at  $0.26 \text{ arcsec min}^{-1}$ , to the fastest moving detection at  $1.55 \text{ arcsec min}^{-1}$ . Generally, we need an object to move at least 2 pixels in order to be detected in our search. Given a pixel scale of  $0.9 \text{ arcsec pixel}^{-1}$  and the longest observing run of 13 h for this data set, we can detect objects moving linearly as slow as  $0.003 \text{ arcsec min}^{-1}$ .

<sup>5</sup><https://ssd-api.jpl.nasa.gov/doc/sbdb.html> (Accessed 31 May 2023)

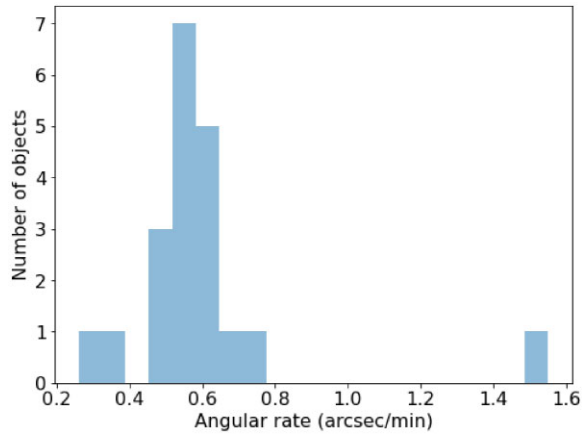


**Figure 3.** Total apparent angular rate in the plane-of-sky distribution for known objects detected in the 2021 ASTEP data.

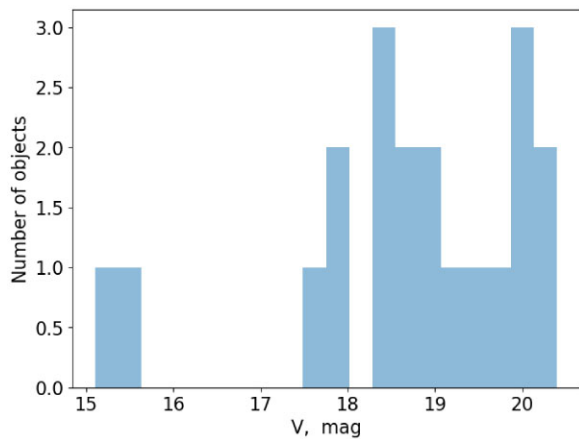


**Figure 4.**  $V$  mag distribution of known objects detected in the 2021 ASTEP data.

The  $V_{\text{mag}}$  of the detected objects ranges from 15.1 mag for the brightest object and 20.4 mag for the faintest. The median  $V_{\text{mag}}$  of the detected objects is 18.9 mag. The faintest detected object with a  $V_{\text{mag}}$  of 20.4 is the MBA 2004 XG58. It was detected on 20 April 2021 with an angular rate of  $0.5 \text{ arcsec min}^{-1}$  and position angle of  $296.7 \text{ deg}$ . The shifted and stacked image is presented in Fig. 5. It is composed of 50 images with exposure times of 120 s from the TOI-772 target field.

To assess efficiency of the pipeline, we compared detected known small bodies with those predicted to be within an FoV at the time of observations, as well as injection-retrieval tests. We used the NASA JPL Small-Body Identification API to obtain small bodies' orbits (which were numerically integrated using a high-fidelity force model). According to the ephemerides, 39 small bodies were present in the FoVs with speeds in the  $0.1\text{--}2.0 \text{ arcsec min}^{-1}$  range and brightness ranging from  $V = 17.5 \text{ mag}$  to  $V = 25.0 \text{ mag}$  (with a median value  $V = 21.5 \text{ mag}$ ). Our pipeline was able to detect 80 per cent of all possible known objects down to  $V = 20.0 \text{ mag}$ . No Near-Earth Asteroids (NEAs) were present in the FoVs. This result is in agreement with the injection-retrieval tests where objects with speed of  $0.2 \text{ arcsec min}^{-1}$  were injected (see Fig. 6). Most of the undetected known objects were too faint or spent too little time with the FoVs to be detected.

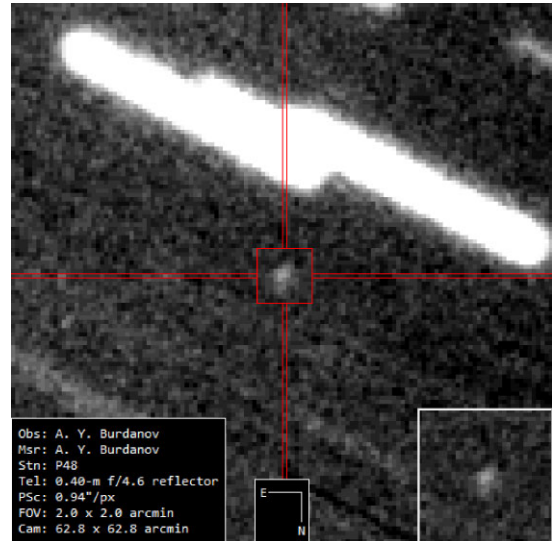


**Figure 5.** Detection of the faintest known object in the data. 2004 XG58 is an MBA detected with a magnitude of  $V = 20.4 \text{ mag}$  and an angular rate of  $0.5 \text{ arcsec min}^{-1}$  on 2021 April 20. The shifted and stacked image is composed of 50 images, each with an exposure time of 120 s in the TOI-772 field.

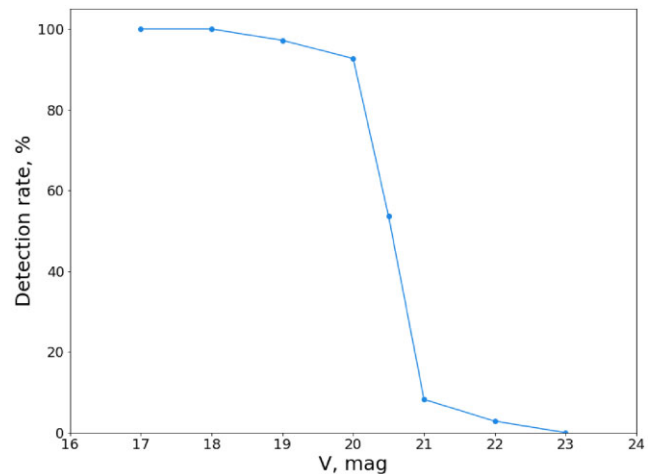


**Figure 6.** Injection-retrieval tests for slow-moving targets ( $0.2 \text{ arcsec min}^{-1}$ ) performed on the data obtained in target field TOI-772 from 20 April 2021.

We did not detect any unknown objects in our search. We attribute non-detections to the location of the target fields probed by the ASTEP project and its limiting magnitude. Most target fields are not located near the ecliptic, which is where the highest concentration of MBAs and Near-Earth objects is located (Morbidelli et al. 2015; Nesvorný 2018). As one moves away from the ecliptic, the detection probability decreases. The majority of the target fields in this survey are located far from the ecliptic, concentrating around  $60 \text{ deg}$  in declination (see Fig. 2). We expect the number of detected objects would be higher if the target fields were located nearer to the ecliptic (e.g. within  $20 \text{ deg}$ ). Another important factor contributing to the number of object detections is that the Southern sky (including high ecliptic latitudes) was extensively searched down to magnitude  $\sim 20$  by several surveys, such as Siding Spring Survey (Larson et al. 2003) and ATLAS (Tonry et al. 2018), while ASTEP's limiting magnitude is  $\sim 20.4 \text{ mag}$ .

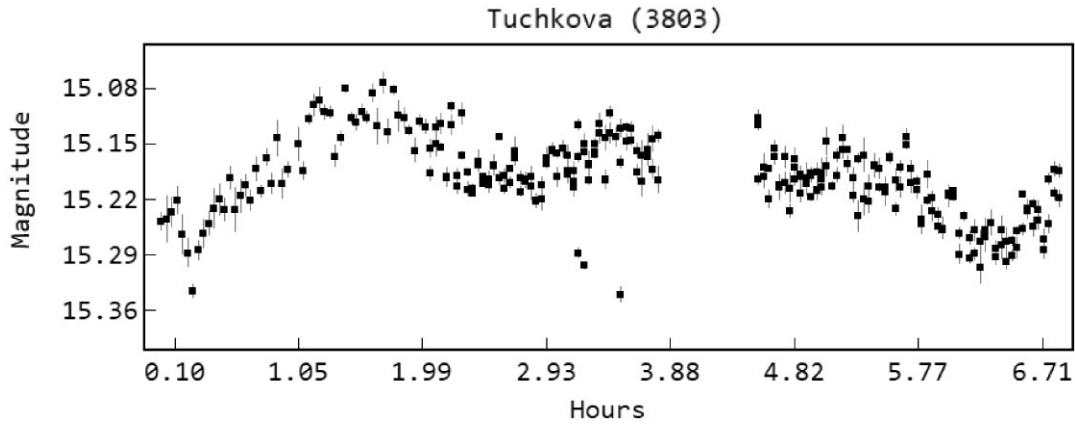


**Figure 7.** Light curve of a known object recovered in observations from 09 April 2021. The known object is main-belt asteroid Tuchkova (3803). It has a median  $V_{\text{mag}}$  of 15.5. The gap in observations around 4 h corresponds to the object’s passing in front of a background star.

In future work, we will apply the pipeline to archival data from the ASTEP project that was obtained during 2010–2013. The data presented in this paper was obtained primarily to confirm candidate transiting exoplanets identified by *TESS*, which resulted in an average observation time of  $\sim 4$  h per target and a maximum observation time of almost 13 h. Previous ASTEP observation strategies (e.g. observations from 2010 to 2013) observed target fields for periods of time longer than a few hours and over the course of many days (Mékarnia et al. 2016). Such extended observations will allow us to treat the data as deep-drilling sets to reach fainter limiting magnitudes than  $V = 20.4$  mag and search for more slowly moving objects, similar to the archival data treatment in B23. For example, the WASP-19 field was observed by ASTEP for 24 nights during May 2010 (Abe et al. 2013). If we were to combine images from 150 h of observations over the course of several nights, we would have the potential to reach a limiting magnitude of  $V = 23$ –24 mag for slow-moving objects that remain in the FoV.

In terms of searching for ISOs in the data near the solar antiapex, the 2021 data included very few fields covering that region from 2021 (see Fig. 1). The known ISO ‘Oumuamua (11/2017 U1) was detected with a magnitude of 19.8, at a heliocentric distance of 1.21 au, and with an on-sky speed of  $\sim 15$  arcsec/min<sup>6</sup> (Bannister et al. 2017; IAU Minor Planet Center 2017). 2I/Borisov (C/2019 Q4) was detected with a magnitude of 17.8, at a heliocentric distance of 2.84 au, and with an on-sky speed of 1.178 arcsec/min<sup>6</sup> (IAU Minor Planet Center 2019; Guzik et al. 2020). These parameters fall within the limitations of our search, meaning ASTEP has the capacity to recover similar ISOs should any cross the FoVs in additional data sets.

We also constructed photometric light curves for the detected known objects. Light curves can provide detailed information about the physical properties and compositions of small bodies. TYCHO TRACKER maintains the capability to construct light curves of any detected objects. The light curve for the MBA Tuchkova (3803) is shown in Fig. 7. Tuchkova is the brightest of the objects detected, with a magnitude of 15.1. The light curves of the remaining object detections be found in the Appendix (Fig. A1) and at the Asteroid Lightcurve Data Exchange Format (ALCDEF) data base (Warner, Harris & Pravec 2009).

The observations of Tuchkova span just under 7 h, with an approximately 45 min gap in the photometry around hour 4 of the

observations (see Fig. 7) due to contamination by a background star. Āurech et al. (2020) report Tuchkova to have a sidereal rotation period of 6.07014 h (Asteroid Lightcurve Database, LCBD; Warner et al. 2009). Our observations cover an entire rotation period for Tuchkova, minus the background star contamination.

TYCHO TRACKER also offers the capability to determine the rotation periods of objects. We used TYCHO TRACKER’s built-in period search function to find the period of Tuchkova from our photometric measurements. The period search function works by finding the period that minimizes the sum of squared residuals from a curve computed as a least squares fit of a Fourier series. The period search returns a list of possible candidate periods each with their corresponding root mean square error (RMSE), and we select the candidate period of 6.158 h, which has the smallest RMSE.

The rotation period reported by Āurech et al. (2020) was obtained from a model that was generated using 478 photometry measurements gathered by ATLAS (Tonry et al. 2018) across 2016–2018. While the period we recovered with TYCHO TRACKER’s built-in period search is close to the value reported in the literature, our observations only cover  $\sim 7$  h of observations on one night. Ideally, we would have more observations that cover multiple rotation periods to gather a more robust estimate on the rotation period of the object.

We see such densely sampled light curves as one of the main advantages of the ASTEP data over other surveys capable of observing similar parts of the sky. For instance, the Legacy Survey of Space and Time (LSST) at the Vera C. Rubin Observatory (Ivezić et al. 2019) is expected to detect over 5 million new Solar system objects fainter than a magnitude of 16. However, light curves available from LSST will have variable sampling and most of them will be sparse (Schwamb et al. 2018, 2023), making light-curve inversion (a technique used to model the surfaces of rotating objects from their brightness variations) more challenging.

## 5 CONCLUSIONS

We have presented the application of our pipeline originally developed in B23 to search for small bodies in data collected by the ASTEP project. The pipeline performs data processing and serves as a wrapper for the synthetic tracking software, TYCHO TRACKER. We analysed one season’s worth of data collected by the ASTEP400 telescope during the 2021 Austral winter, in an effort to begin maximizing the science return of the survey.

<sup>6</sup><https://ssd.jpl.nasa.gov/horizons> (Accessed 31 May 2023)

In total, 167 target fields with 143 unique targets were observed by the ASTEP400 telescope in 2021, over the course of 216 nights. Of these fields, we processed 206 nights with 141 unique targets after removing defocused target fields. We identified 20 known objects in the data set in 5 fields across 6 nights of observations. The known objects span a few dynamical classes, including 1 inner main-belt asteroid, 18 main-belt asteroids, and 1 comet. Most of the objects were identified in fields near the ecliptic plane, which aligns well with the inclination distribution of small bodies in the Solar system. Object detections were made with no prior assumptions on objects' speed or position angles. After reviewing the candidate detections, we reported them to the MPC. The magnitudes of object detections ranged from  $V = 15.1$  mag to  $V = 20.4$  mag, and the objects' speeds ranged from  $0.26$  arcsec  $\text{min}^{-1}$  to  $1.55$  arcsec  $\text{min}^{-1}$ . We compared detected objects with those known to be present in the FoVs. The objects that were present but undetected were too faint to be recovered, with  $V > 20.0$  mag.

Next steps will include applying the pipeline to archival data from the ASTEP project that was obtained during 2010–2013. These observations were conducted for periods of time longer than a few hours and over the course of many days (Mékarnia et al. 2016), unlike the *TESS* follow-up work. Extended observations will allow us to reach fainter limiting magnitudes than  $V = 20.4$  mag and search for more slowly moving objects.

Our data processing and analysis pipeline can continue to be adapted and applied to other photometric surveys to maximize their science return. The pipeline continues to reduce SPECULOOS data at the time of writing and has the potential to run as a 'last night' process for ASTEP provided there are adequate computing resources at Concordia Station. The reduction of observations taken since December of 2021 would also allow us to obtain color information for any detected small body that crosses the FoV due to the new addition of a camera capable of two-colour photometry on the ASTEP telescope (Schmider et al. 2022).

## ACKNOWLEDGEMENTS

We thank the reviewer, Dr Meg Schwamb, for her time, attention, and constructive criticism. Dr Schwamb's comments helped us to improve the quality of the paper. We thank and acknowledge the vital assistance of the French and Italian polar agencies (IPEV and PNRA), and all their staff, particularly the wintering-over staff of Concordia Station, without whom operations of ASTEP would not be possible. The authors would also like to thank Daniel Parrott, the developer of TYCHO TRACKER, for his advice and assistance with the software.

This research has made use of data and/or services provided by the International Astronomical Union's Minor Planet Center.

*Software:* TYCHO TRACKER ([www.tycho-tracker.com](http://www.tycho-tracker.com), Parrott 2020), ASTROPY (Astropy Collaboration 2013, 2018), NUMPY (Harris et al. 2020), and MATPLOTLIB (Hunter 2007). This research made use of PHOTUTILS, an ASTROPY package for detection and photometry of astronomical sources (Bradley et al. 2023).

This work has been supported by the NVIDIA Academic Hardware Grant Program. This research is supported from the European Research Council (ERC) under the European Union's Horizon 2020 research and innovation programme (grant agreement no. 803193/BEBOP) and from the Science and Technology Facilities Council (STFC; grant no. ST/S00193X/1).

## DATA AVAILABILITY

Photometry of detected objects is available at the ALCDEF data base (Warner, Harris & Pravec 2009). Objects' photometry was uploaded on 2023 August 31 and can be accessed by any user by either downloading the entire ALCDEF table or by performing an object search in the data base. The remaining data are available on request to the corresponding author.

## REFERENCES

- Abe L. et al., 2013, *A&A*, 553, A49  
 Astropy Collaboration, 2013, *A&A*, 558, A33  
 Astropy Collaboration, 2018, *AJ*, 156, 123  
 Bannister M. T. et al., 2017, *ApJ*, 851, L38  
 Bradley L. et al., 2023, astropy/photutils: 1.8.0, available at: <https://doi.org/10.5281/zenodo.7946442>  
 Burdanov A., Hasler S., de Wit J., 2023, *MNRAS*, 521, 4568  
 Burt J. A. et al., 2021, *AJ*, 162, 87  
 Chen C. et al., 2023, *MNRAS*, 520, 4601  
 Crouzet N. et al., 2010, *A&A*, 511, A36  
 Crouzet N. et al., 2011, in European Physical Journal Web of Conferences. EDP Sciences - Web of Conferences, 17, Avenue du Hoggar, Parc d'Activités de Courtabœuf, B.P. 112, F-91944 Les Ulis Cedex A. Vol. 11, France, p. 06001  
 Crouzet N. et al., 2018, *A&A*, 619, A116  
 Crouzet N. et al., 2020, in Evans J. C., Bryant J. J., Motohara K., eds, Proc. SPIE Conf. Ser. Vol. 11447, Ground-based and Airborne Instrumentation for Astronomy VIII. SPIE, Bellingham  
 Daban J.-B. et al., 2010, in Stepp L. M., Gilmozzi R., Hall H. J., eds, Proc. SPIE Conf. Ser. Vol. 7733, Ground-based and Airborne Telescopes III. SPIE, Bellingham  
 DeMeo F. E., Carry B., 2014, *Nature*, 505, 629  
 Delrez L. et al., 2018, in Marshall H. K., Spyromilio J., eds, Proc. SPIE Conf. Ser. Vol. 10700, Ground-based and Airborne Telescopes VII. SPIE, Bellingham, p. 107001I  
 Dones L., Brasser R., Kaib N., Rickman H., 2015, *Space Sci. Rev.*, 197, 191  
 Dransfield G. et al., 2022a, *MNRAS*, 515, 1328  
 Dransfield G. et al., 2022b, in Adler D. S., Seaman R. L., Benn C. R., eds, Proc. SPIE Conf. Ser. Vol. 12186, Observatory Operations: Strategies, Processes, and Systems IX. SPIE, Bellingham, p. 121861F  
 Durand G. A. et al., 2014, in Stepp L. M., Gilmozzi R., Hall H. J., eds, Proc. SPIE Conf. Ser. Vol. 9145, Ground-based and Airborne Telescopes V. SPIE, Bellingham, p. 91450D  
 Ďurech J., Tonyr J., Erasmus N., Denneau L., Heinze A. N., Flewelling H., Vančo R., 2020, *A&A*, 643, A59  
 Gillon M., 2018, *Nature Astron.*, 2, 344  
 Grec G., Fossat E., Pomerantz M., 1980, *Nature*, 288, 541  
 Guillot T. et al., 2015, *Astron. Nachr.*, 336, 638  
 Guzik P., Drahus M., Rusek K., Waniak W., Cannizzaro G., Pastor-Marazuela I., 2020, *Nature Astron.*, 4, 53  
 Gwyn S. D. J., Hill N., Kavelaars J. J., 2012, *PASP*, 124, 579  
 Harris C. R. et al., 2020, *Nature*, 585, 357  
 Høg E. et al., 2000, *A&A*, 357, 367  
 Hoover D. J., Seligman D. Z., Payne M. J., 2022, *Planetary Sci. J.*, 3, 71  
 Hromakina T. et al., 2021, *A&A*, 647, A71  
 Hunter J. D., 2007, *Comput. Sci. Eng.*, 9, 90  
 IAU Minor Planet Center, 2017, MPEC 2017-U183: A/2017 U1, available at: <https://minorplanetcenter.net/mpec/K17/K17UI3.html>  
 IAU Minor Planet Center, 2019, MPEC 2019-R106: Comet C/2019 Q4 (Borisov), available at: <https://www.minorplanetcenter.net/mpec/K19/K19RA6.html>  
 Indermuehle B. T., Burton M. G., Maddison S. T., 2005, *PASA*, 22, 73  
 Ivezić Ž. et al., 2019, *ApJ*, 873, 111  
 Jehin E. et al., 2018, *Messenger*, 174, 2  
 Larson S., Beshore E., Hill R., Christensen E., McLean D., Kolar S., McNaught R., Garradd G., 2003, in AAS/Division for Planetary Sciences



- Meeting Abstracts #35. Vol. 35. American Astronomical Society/Division of Planetary Sciences. Monterey, CA, p. 36.04
- Meech K. J. et al., 2017, *Nature*, 552, 378
- Mékarnia D. et al., 2016, *MNRAS*, 463, 45
- Michel P., DeMeo F. E., Bottke W. F., 2015, *Asteroids IV*, 1, 1
- Morbidelli A., Walsh K. J., O'Brien D. P., Minton D. A., Bottke W. F., 2015, in *Asteroids IV*. Univ. Arizona Press, p. 493
- Nesvorný D., 2018, *ARA&A*, 56, 137
- Parrott D., 2020, *J. Am. Assoc. Variable Star Obs.*, 48, 262
- Pomerantz M., Wyller A., Kusoffsky U., 1981, in Dunn R. B., ed., *Solar Instrumentation: What's Next?*. Conference Proceedings. Sacramento Peak National Observatory, Sunspot, NM, p. 379
- Schmider F.-X. et al., 2022, in Marshall H. K., Spyromilio J., Usuda T., eds, *Proc. SPIE Conf. Ser. Vol. 12182, Ground-based and Airborne Telescopes IX*. SPIE, Bellingham, p. 121822O
- Schwamb M. E. et al., 2018, preprint([arXiv:1802.01783](https://arxiv.org/abs/1802.01783))
- Schwamb M. E. et al., 2023, *ApJS*, 266, 22
- Tonry J. L. et al., 2018, *PASP*, 130, 064505
- Tosti G., Busso M., Ciprini S., Persi P., Ferrari-Toniolo M., Corcione L., 2003, *Mem. Soc. Astron. Italiana*, 74, 37
- Trifonov T. et al., 2023, *AJ*, 165, 179
- Vaduvescu O., Curelaru L., Birlan M., Bocsa G., Serbanescu L., Tudorica A., Berthier J., 2009, *Astron. Nachr. Astron. Notes*, 330, 698
- Vaduvescu O., Curelaru L., Popescu M., 2020, *Astron. Comput.*, 30, 100356
- Warner B. D., Harris A. W., Pravec P., 2009, *Icarus*, 202, 134
- Yuan X. et al., 2014, in Stepp L. M., Gilmozzi R., Hall H. J., eds, *Proc. SPIE Conf. Ser. Vol. 9145 Ground-based and Airborne Telescopes V*. SPIE, Bellingham, p.91450F

## SUPPORTING INFORMATION

Supplementary data are available at [MNRAS](https://www.mnras.org/) online.

### suppl\_data

Please note: Oxford University Press is not responsible for the content or functionality of any supporting materials supplied by the authors. Any queries (other than missing material) should be directed to the corresponding author for the article.

## APPENDIX: LIGHT CURVES OF DETECTED OBJECTS

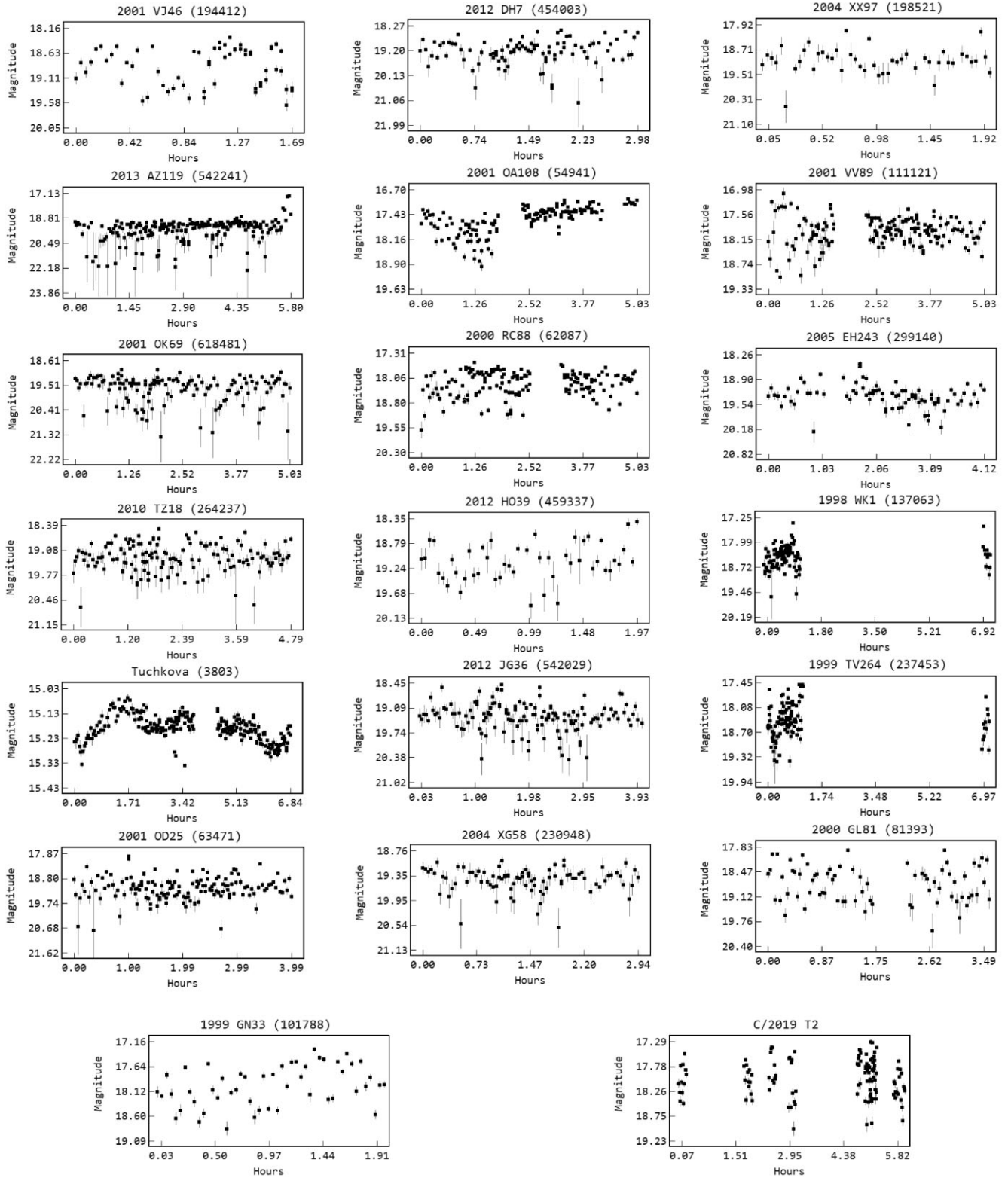


**Figure A1.** Light curves of all detected objects from the 2021 ASTEP data. Magnitude refers to apparent magnitude of the objects.

This paper has been typeset from a  $\text{\TeX}/\text{\LaTeX}$  file prepared by the author.